# Statistical properties and geoefficiency of interplanetary coronal mass ejections and their sheaths during intense geomagnetic storms

Jianpeng Guo,[1] Xueshang Feng,[1] Jie Zhang,[2] Pingbing Zuo,[1] and Changqing Xiang[1]

Received 26 November 2009; revised 22 March 2010; accepted 31 March 2010; published 16 September 2010.

[1] In this paper, we examine and compare the statistical properties of interplanetary coronal mass ejections (ICMEs) and their sheath regions in the near-Earth space, mainly focusing on the distributions of various physical parameters and their geoefficiency. The 53 events studied are a subset of events responsible for intense ($Dst \leq -100$ nT) geomagnetic storms during the time period from 1996 to 2005. These events all fall into the single-type category in which each of the geomagnetic storms was caused by a well-isolated single ICME, free of the complexity of the interaction of multiple ICMEs. For both sheaths and ICMEs, we find that the distributions of the magnetic field strength, the solar-wind speed, the density, the proton temperature, the dynamic pressure, the plasma beta, and the Alfvén Mach number are approximately lognormal, while those of the $Bz$ component and the $Y$ component of the electric field are approximately Gaussian. On the average, the magnetic field strengths, the $Bz$ components, the speeds, the densities, the proton temperatures, the dynamic pressures, the plasma betas, and the Mach numbers for the sheaths are 15, 80, 4, 60, 70, 62, 67, and 30% higher than the corresponding values for ICMEs, respectively, whereas the $Y$ component of the electric field for the sheaths is almost 1 s of that for ICMEs. The two structures have almost equal energy transfer efficiency and comparable Newell functions, whereas they show statistically meaningful differences in the dayside reconnection rate, according to the Borovsky function.

**Citation:** Guo, J., X. Feng, J. Zhang, P. Zuo, and C. Xiang (2010), Statistical properties and geoefficiency of interplanetary coronal mass ejections and their sheaths during intense geomagnetic storms, *J. Geophys. Res.*, *115*, A09107, doi:10.1029/2009JA015140.

## 1. Introduction

[2] Manifestations of coronal mass ejections (CMEs) from the Sun are frequently observed in the solar wind near the Earth and are commonly called interplanetary coronal mass ejections (ICMEs). The signatures of ICMEs have been discussed extensively, such as low-proton temperature, enhanced magnetic field strength, high ratio of alpha to proton particles, and bidirectional electron heat flux [e.g., *Richardson and Cane*, 1995; *Neugebauer and Goldstein*, 1997; *Richardson and Cane*, 2004; *Owens et al.*, 2005; *Wimmer-Schweingruber et al.*, 2006; *Zurbuchen and Richardson*, 2006]. However, there is no single signature or a combination of signatures that is a foolproof ICME identifier. ICMEs are also called ejecta, which could be either magnetic clouds (MCs) or noncloud ejecta. MCs are defined as having a smooth magnetic field rotation (interpreted as a morphology of magnetic flux rope) and enhanced magnetic field magnitude coupled with a reduced proton temperature [*Burlaga et al.*, 1981], and they comprise somewhere between one third to one half [*Cane and Richardson*, 2003] of all ICMEs observed at 1 AU [*Gosling*, 1990; *Cane and Richardson*, 2003; *Riley et al.*, 2006]. ICMEs moving faster than the ambient solar wind will compress and deflect the upstream flow. If the relative speed of the two plasma regimes is greater than the fast mode magnetohydrodynamic wave speed, then a shock will form ahead of the ICME. The region of compressed solar wind bounded by the leading shock front and the trailing ICME leading edge is referred to as the sheath region. The sheath regions often have highly fluctuating fields, density, and dynamic pressure. The boundary between the trailing edge of the sheath and the ICME can sometimes be difficult to identify. This may be partly due to the dynamic nature of ICME propagation and, possibly, to evolution with time, e.g., by reconnection [e.g., *Gosling et al.*, 2005]. Moreover, different in situ signatures do not necessarily give the same boundaries. The primary objective of the present study is to examine and compare the distributions of the variables in these two different regions: sheaths and ICMEs. The variables we chose include the characteristic quantities of solar wind as well as the geoeffective parameters. They are (1) the magnetic field strength $B$, (2) the $Bz$ component, (3) the solar-wind velocity $V$, (4) the solar-wind density $N$, (5) the proton

[1]SIGMA Weather Group, State Key Laboratory of Space Weather, Center for Space Science and Applied Research, Chinese Academy of Sciences, Beijing, China.
[2]Department of Computational and Data Sciences, George Mason University, Fairfax, Virginia, USA.


0148-0227/10/2009JA015140

temperature *Tp*, (6) the dynamic pressure *Pdy*, (7) the *Y* component of the electric field *Ey*, (8) the plasma beta $\beta$, and (9) the Alfvén Mach number $M_A$. A statistical knowledge of these important parameters will help us understand the solar-wind properties.

[3] The solar-wind parameters largely control the solar-wind–magnetospheric coupling, although the magnetospheric behavior also has some control [*Borovsky*, 2008; *Borovsky et al.*, 2008]. Thus, the differences in the geoefficiency between different types of interplanetary structures, such as ICMEs and sheaths, should be expected. Within a sheath, the dynamic pressure is typically high and more fluctuating, and the magnetic field direction can change several times from south to north while, during an ICME, the magnetic field direction typically changes smoothly over the time-scales of a day [*Huttunen et al.*, 2008]. Furthermore, the passages of sheath regions are usually short in duration, because their radial sizes are smaller when compared to that of corresponding ICMEs. According to *Zhang et al.* [2008], the durations and radial sizes of the ICMEs range from 8.0 to 62.0 h and 0.08 to 0.63 AU, respectively, with average values of 30.6 h and 0.37 AU. The sheath durations and radial sizes range from 2.6 to 24.5 h and 0.03 to 0.31 AU, respectively, with average values of 10.6 h and 0.13 AU. For MCs, their durations range from a few hours to more than 40 h, with an average value of 20.5 h, and the temporal separation between the shock and MC arrivals averages to 12.1 h [*Lepping et al.*, 2006; *Gopalswamy*, 2006; *Gopalswamy et al.*, 2008]. The larger size of ICMEs in *Zhang et al.*'s [2008] study is likely a selection effect due to the fact that the events used in the study produced major geomagnetic storms and, thus, may possess a larger physical size that may help to sustain the geoeffective solar-wind condition. From both forecasting and basic physics viewpoints, there is a need for a better understanding of the solar-wind–magnetosphere system during the two solar-wind structures. The second objective of the present study is to investigate the interaction of the two solar-wind structures with the magnetosphere, using solar-wind–magnetosphere coupling functions.

## 2. Observations

[4] The ICMEs used in this study are a subset of the 88 events that produced intense ($Dst \leq -100$ nT) geomagnetic storms during the period of 1996–2005 [*Zhang et al.*, 2007]. For the purpose of this study, we selected only the 53 so-called "S-type" events. Of the S-type storms, *Zhang et al.* [2008] selected 46 events, for which data are available from the Advanced Composition Explorer (ACE) spacecraft, to study the sizes of the ICME and sheath. The 53 events all fall into the single-type category, in which each of the geomagnetic storms was caused by a well-isolated single ICME in the near-Earth space, free of the complexity of the interaction of multiple ICMEs. The corresponding solar-wind magnetic field and plasma parameters are available from the 5 min averaged OMNI database (spacecraft-interspersed, near-Earth solar wind data) at 1 AU (geocentric solar magnetospheric coordinates).

[5] For each of the 53 events, we identified three critical times:

[6] 1. The first is the arrival time of the ICME-driven shock (or wave) giving the start time of the sheath.

[7] 2. The second is the ICME arrival time, also indicating the trailing edge of the sheath.

[8] 3. The third is the ICME ending time.

[9] The shock/wave arrival time is obtained from examining the solar-wind data upstream of the ICME for sharp discontinuities or more gradual increases in the solar-wind speed, temperature, density, and magnetic field intensity. We also referred to the ACE shock list (http://www.ssg.sr.unh.edu/mag/ace/ACElists/obs_list.html) and considered the transit time for the shock from the ACE spacecraft to the magnetopause. Several recent studies have focused on interplanetary shocks [*Howard and Tappin*, 2005; *Oh et al.*, 2007; *Gopalswamy et al.*, 2010]. Note that preceding disturbances driven by slower ICMEs may not have steepened into shocks at 1 AU. To identify the start and end times of the ICME, we have used a combination of ICME signatures, including an enhancement of the magnetic field with a smooth rotation through a large angle, low-field variance, abnormally low proton temperature, and enhanced oxygen and iron charge states [*Wimmer-Schweingruber et al.*, 2006; *Zurbuchen and Richardson*, 2006]. We also refer to an updated version of the "comprehensive" ICME list compiled by *Cane and Richardson* [2003] that also considers additional ICME signatures: in particular, solar-wind ion composition and charge state anomalies [*Lepri et al.*, 2001; *Richardson and Cane*, 2004]. The updated list is available at http://www.ssg.sr.unh.edu/mag/ace/ACElists/ICMEtable.html. We find that, although most of the signatures generally indicate a consistent starting time for a CME, the ending time may be less well defined. In this situation, for consistency, we use the trailing edge of the enhanced and smooth magnetic field to define the ending time of the ICME. Once the ICME region boundaries are identified, it is straightforward to collect all the solar-wind parameter points every 5 min for the sheaths and ICMEs, and use all of them (combined for all 53 events) for present statistical analysis.

## 3. Distributions of the Sheath and Interplanetary Coronal Mass Ejection Variables

[10] The statistical probability distributions of the variables of both sheaths and ICMEs are shown in Figure 1. The two curves in each panel are the fits of the distributions to a lognormal probability density function, except for *Bz* and *Ey*, which are fits to a Gaussian probability density function for the sheath regions (solid) and the ICMEs (dashed), respectively. The lognormal probability density function [*Mood et al.*, 1974] of a variable $x$ is

$$f(x;\mu,\sigma) = \frac{1}{x\sigma\sqrt{2\pi}} e^{-(\ln x-\mu)^2/2\sigma^2} \quad (1)$$

where the parameters $\mu$ and $\sigma$ are the mean and the standard deviation of the variable's natural logarithm, respectively. The Gaussian probability density function [*Whang*, 1977] is

$$f(x;\mu,\sigma) = \frac{1}{\sigma\sqrt{2\pi}} e^{-(x-\mu)^2/2\sigma^2} \quad (2)$$

where the parameters $\mu$ and $\sigma$ are the mean and the standard deviation of the variable, respectively. For lognormal (Gaussian) fit, $\mu$ is the most probable value of the variable's

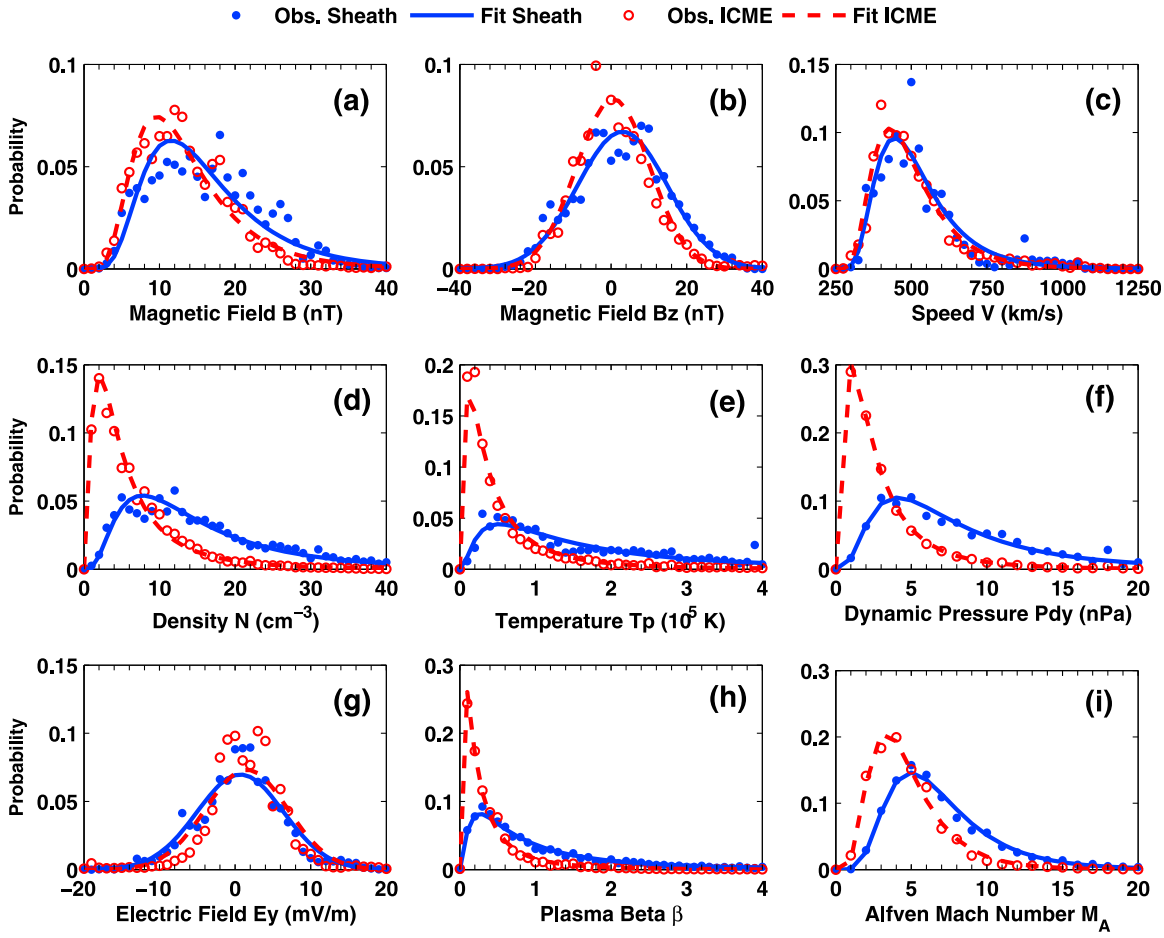


**Figure 1.** Distributions of various solar-wind parameters in sheath regions (plus symbols with solid curves) and ICMEs (asterisk symbols with dashed curves). The parameters include (a) the magnetic field strength $B$, (b) the $Bz$ component, (c) the solar-wind velocity $V$, (d) the solar-wind density $N$, (e) the proton temperature $Tp$, (f) the dynamic pressure $Pdy$, (g) the $Y$ component of the electric field $Ey$, (h) the plasma beta $\beta$, and (i) the Alfvén Mach number $M_A$. The distribution profiles are well fitted with a lognormal distribution function, except for $Bz$ and $Ey$, which are fit with a Gaussian function.

natural logarithm (the variable), and $\sigma$ shows how much variation there is from the mean. Note that Bz and Ey have negative or positive values in the solar wind; we take a cutoff (250 km/s) for $V$. Table 1 lists the corresponding estimates of the mean and standard deviation of the formula fittings for the variables (columns 3 to 6); the high correlations ($r$, columns 7 to 8) confirmed the goodness of the lognormal or Gaussian fit to the distributions of these variables [e.g., *Burlaga and Ness*, 1998; *Padhye et al.*, 2001]; the last two columns indicate their mean physical values. As we can see from Figure 1, the distributions of $B$, $V$, $N$, $Tp$, $Pdy$, $\beta$, and $M_A$ for both sheaths and ICMEs are lognormal

**Table 1.** Parameters $\mu$, $\sigma$ and Correlations $r$ Obtained From the Probability Density Function Fit (Lognormal Distribution or Gaussian Distribution) for the Variables of the Sheaths and ICMEs, Together With the Average Values of These Variables[a]

| Solar-Wind Parameters | Distribution Function | $\mu$ | | $\sigma$ | | $r$ | | Mean | |
|---|---|---|---|---|---|---|---|---|---|
| | | Sheath | ICME | Sheath | ICME | Sheath | ICME | Sheath | ICME |
| $B$ (nT) | Lognormal | 2.69 | 2.51 | 0.49 | 0.49 | 0.90 | 0.96 | 16.35 | 13.83 |
| $Bz$ (nT) | Gaussian | 3.02 | 0.58 | 11.89 | 9.60 | 0.97 | 0.95 | 3.02 | 0.58 |
| $V$ (km/s) | Lognormal | 2.28 | 2.20 | 0.47 | 0.49 | 0.93 | 0.98 | 524 | 503 |
| $N$ (cm$^{-3}$) | Lognormal | 2.58 | 1.53 | 0.73 | 0.92 | 0.95 | 0.99 | 16.90 | 6.76 |
| $Tp$ (10$^5$ K) | Lognormal | 2.71 | 1.35 | 1.03 | 1.08 | 0.91 | 0.98 | 2.56 | 0.75 |
| $Pdy$ (nPa) | Lognormal | 1.92 | 0.79 | 0.72 | 0.89 | 0.97 | 0.99 | 8.76 | 3.28 |
| $Ey$ (mV/m) | Gaussian | 0.69 | 1.52 | 5.72 | 5.44 | 0.96 | 0.94 | 0.68 | 1.50 |
| $\beta$ | Lognormal | 2.08 | 0.87 | 1.07 | 1.15 | 0.99 | 0.99 | 1.52 | 0.50 |
| $M_A$ | Lognormal | 1.84 | 1.45 | 0.49 | 0.51 | 0.99 | 0.99 | 7.12 | 4.90 |

[a]Average $Bz$ and $Ey$ values refer to their arithmetic values.

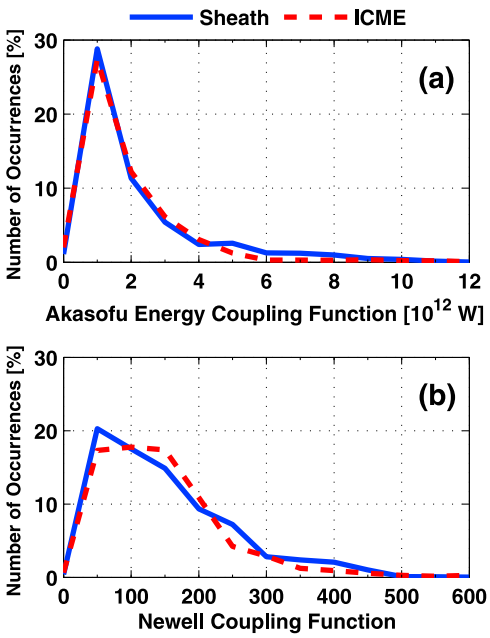


**Figure 2.** (a) Normalized occurrence distributions (in percentage) of the *Akasofu* [1981] function and (b) the Newell function [*Newell et al.*, 2007], for both the sheaths (solid curves) and the ICMEs (dashed curves).

to a good approximation. The distributions of $V$ for the sheaths and ICMEs are almost identical, whereas the tails of the distributions of $B$, $N$, $Tp$, $Pdy$, $\beta$, and $M_A$ are apparently longer for ICMEs. The distributions of the $Bz$ component and the $Y$ component of the electric field for both sheaths and ICMEs reveal an approximately Gaussian distribution ranging from −40 to 40 nT and −20 to 20 mV/m, respectively, although there is possibly a small excess of low-electric fields.

[11] We further calculate the mean physical values of the variables of both sheaths and ICMEs, and the results are also listed in the last two columns of Table 1. Note that the average $Bz$ and $Ey$ values refer to their arithmetic values. The average $B$ in the sheaths is 16.35 nT, compared to 13.83 nT for ICMEs, and both are significantly higher than the long-term average value of 6 nT for the solar wind [*Burlaga et al.*, 2001]. According to *Gopalswamy* [2008], the average $B$ (note that here, $B$ corresponds to the maximum value in the ICME interval) is about 23.1 and 19.8 nT for MCs and non-MCs, respectively. The average $Bz$ component for sheaths is 3.02 nT, compared to 0.58 nT for ICMEs. The average $Bs$ (the negative component of $Bz$) for sheaths is −8.48 nT, compared to −6.37 nT for ICMEs. The average $V$ for the sheaths (524 km/s) is comparable to that for ICMEs (503 km/s). The average $V$ is 559 km/s for MCs, compared to 636 km/s for non-MCs [*Gopalswamy*, 2008] [note that here, $V$ corresponds to the speed at the time of MC arrival and the maximum speed within the ICME interval for MCs and non-MCs, respectively]. *Owens et al.* [2005] investigated the relation between the characteristic magnetic field strengths and speeds of both MCs and non-MCs at 1 AU and found that correlation between field and speed is only significant in the sheath region ahead of MCs, not within MCs themselves, whereas such a relation is not revealed in the sheaths ahead of non-MCs. The average $N$ for the sheaths is 16.90 $cm^{-3}$, compared to 6.76 $cm^{-3}$ for ICMEs, and the latter is comparable to the long-term average value for the solar wind (7 $cm^{-3}$) [*Liu et al.*, 2005]. The average $Tp$ in the sheaths is $2.56 \times 10^5$ K, compared to $1.41 \times 10^3$ K for ICMEs; these averages are higher and lower, respectively, than the long-term average value for the solar wind of $1.50 \times 10^5$ K [*Burlaga et al.*, 2001]. The average $Pdy$ in the sheaths is 8.76 nPa, compared to 3.28 nPa for ICMEs. The arithmetic average $Ey$ for ICMEs (1.50) is twice that for sheaths (0.68) (see also the range of X values in Figures 17h and 17p of *Gopalswamy*'s [2008] paper). The average $\beta$ for sheaths (1.52) is about three times that (0.5) for ICMEs. The average $M_A$ in the sheaths is 7.12, compared to 4.90 for ICMEs, and both are lower than the long-term average value for the solar wind of about 7.5 [*Lavraud and Borovsky*, 2008]. It should be noted that the Alfvénic Mach numbers in this study are provided by the OMNI data set and are not computed in the solar-wind frame. More recent study shows that the computed average values for the shock Mach numbers at 1 AU is about 3.2 in the solar-wind frame [*Gopalswamy et al.*, 2010].

## 4. Coupling Efficiency of the Sheaths and Interplanetary Coronal Mass Ejections With the Magnetosphere

[12] To investigate the coupling efficiency of both sheaths and ICMEs with the magnetosphere, we use two types of solar-wind–magnetosphere coupling functions, namely, the solar-wind "driver function" and the solar-wind "control function" (cf., *Borovsky*, 2008). The driver functions are derived with "tuning" to optimize correlation coefficients between magnetospheric measurements and solar-wind measurements, while there are no explicit free parameters in the control function.

### 4.1. Solar-Wind Driver Function

[13] The solar-wind driver functions used are the well-known Akasofu function (or the epsilon parameter) (Equation 3) [*Akasofu*, 1981] and the Newell formula (Equation 4) [*Newell et al.*, 2007]:

$$\varepsilon(W) = \frac{4\pi}{\mu_0} v B^2 \sin^4\left(\frac{\theta}{2}\right) l_0^2 \tag{3}$$

$$d\Phi/dt = v^{4/3} B_T^{2/3} \sin^{8/3}\left(\frac{\theta}{2}\right) \tag{4}$$

The variables $v$, $B$, $B_T$, $\theta$, and $l_0$ on the right-hand side denote the solar-wind velocity, the solar-wind magnetic field magnitude, the solar-wind magnetic field perpendicular to the Sun–Earth line, the interplanetary magnetic field (IMF) clock angle, and the scaling factor. The factor $l_0$ is the linear dimension of an "effective cross-sectional area" of the magnetosphere determined empirically to $l_0 = 7\ R_E$ [*Perreault and Akasofu*, 1978]. The epsilon parameters for both the sheaths and ICMEs are shown in fractional bins in Figure 2 (a). As we can see, the normalized occurrence distributions (in percentage) of the sheaths and ICMEs are

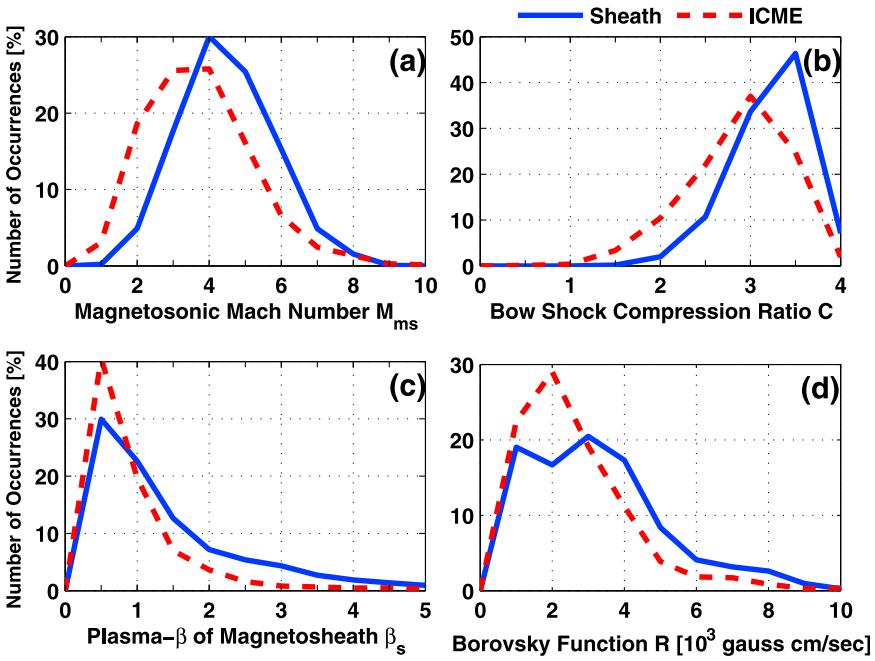


**Figure 3.** Normalized occurrence distributions (in percentage) of (a) the magnetosonic Mach number $M_{ms}$, (b) the bow shock compression ratio $C$, (c) the plasma $\beta$ of the magnetosheath, and (d) the Borovsky function for the sheaths (solid curves) and the ICMEs (dashed curves).

almost overlapping with each other. The average value for the sheaths is $1.41 \times 10^{12}$ K, compared to $1.34 \times 10^{12}$ K for the ICMEs. Therefore, the energy transfer efficiencies for the sheaths and ICMEs are quite comparable. Similarly, the Newell function for both the sheaths and ICMEs is shown in fractional bins in Figure 2 (b). There are very few visible differences between the occurrence distributions of the sheaths and the ICMEs. The average Newell parameter for the sheaths (122) is comparable to that for the ICMEs (116). Interestingly, the difference between the two components is not statistically distinguishable for the coupling efficiency calculated from both driving functions.

### 4.2. Solar-Wind Control Function

[14] The solar-wind control function used is the Borovsky function [*Borovsky*, 2008], (i.e., a reconnection rate written in terms of upstream solar-wind parameters):

$$R = 0.4\mu_0^{1/2}\sin(\theta/2)\rho v^2\left(1+0.5M_{ms}^{-2}\right)(1+\beta_s)^{-1/2} \cdot \left[C\rho + (1+\beta_s)^{-1/2}\rho_m\right]^{-1/2}\left[(1+\beta_s)^{1/2}+1\right]^{-1/2} \quad (5)$$

where

$$\beta_s = 3.2\times 10^{-2} M_A^{1.92} \quad (6)$$

is the plasma $\beta$ of the magnetosheath near the nose of the magnetosphere,

$$C = \{[1/4]^6 + [1/(1+1.38\log_e(M_A))]^6\}^{-1/6} \quad (7)$$

is the compression ratio of the bow shock,

$$M_{ms} = v/((B/4\pi\rho)+2P/\rho)^{1/2} \quad (8)$$

is the magnetosonic Mach number of the solar wind, and

$$M_A = v(4\pi\rho)^{1/2}/B \quad (9)$$

is the Alfvén Mach number of the solar wind. A term $\sin(\theta/2)$ is also added to account for the component reconnection when the IMF has a clock angle of $\theta$. In these expressions, $v$, $\rho$, $B$, and $P$ are the speed, mass density, magnetic field strength, and particle pressure (thermal plus kinetic) in the upstream solar wind. The Borovsky function is based on the idea that dayside reconnection is governed by local plasma parameters and that whatever controls those parameters controls the reconnection rate. The physical interpretation of the control function is that solar-wind pressure $\rho v^2(1 + 0.5M_{ms}^{-2})$ largely controls the reconnection rate, essentially by setting the strength of the magnetic field at the nose of the magnetosphere via pressure balance.

[15] The magnetosonic Mach number $M_{ms}$ sets the properties of the Earth's bow shock, which converts unshocked solar-wind plasma into shocked magnetosheath plasma. The magnetosonic Mach number controls the compression ratio $C$ of the shock, which is the multiplicative density change from upstream to downstream. The compression ratio $C$ varies from 1 to 4 [*Tidman and Krall*, 1971]. In solar-wind–magnetosphere coupling, it is actually the magnetosheath flow that drives activity in the Earth's magnetosphere, and the bow shock converts solar-wind flow into magnetosheath flow [*Borovsky and Denton*, 2006; *Lavraud and Borovsky*, 2008]. The magnetosonic Mach number $M_{ms}$, the bow shock compression ratio $C$, the plasma $\beta$ of the magnetosheath, and the Borovsky function for both the sheaths and the ICMEs are shown in fractional bins in Figures 3a, 3b, 3c, and 3d, respectively. In calculating the magnetosonic Mach number,

the electron temperature $1.5 \times 10^5$ K is taken for the solar wind, since measurements of Te are not available in the OMNI database. In fact, the solar-wind electron temperature is relatively constant when compared to the proton temperature, and it is not influenced by other concurrent parameters in the solar wind [*Newbury et al.*, 1998]. Moreover, $Te = 1.5 \times 10^5$ K is approximately valid for all types of solar wind [*Skoug et al.*, 2000]. In addition, we take $\rho_m = 0$ in expression (5) due to no information about the dayside magnetospheric mass density $\rho_m$. As we can see from Figure 3, the magnetosonic Mach numbers for the sheaths are, in general, larger than those for ICMEs, with average values of 4.5 and 3.7, respectively. Similarly, the compression ratio $C$ is also larger for the sheath regions, with an average value of 3.2 when compared with that of ICMEs with an average value of 2.9. In about 49% of the time, the sheath region has low $\beta_s < 1$ in the magnetosheath, whereas, in about 76% of the time, the ICME has low $\beta_s < 1$. Unlike the driving functions, the Borovsky parameter shows a clear difference between the sheaths and ICMEs, with an average value of $3.3 \times 10^3$ and $2.6 \times 10^3$ gauss cm/s, respectively. A t test was done to test the significance of the differences, and the P value of $1.05 \times 10^{-8}$ indicates that the average values are statistically different (note that any value of P less than 0.05 gives greater than 95% confidence that they are statistically different). This indicates a higher degree of coupling efficiency for the sheaths.

## 5. Summary and Discussions

[16] We have shown that the distribution functions of the magnetic field strength, the solar-wind speed, the density, the proton temperature, the dynamic pressure, the plasma beta, and the Alfvén Mach number are approximately lognormal, while those of the *Bz* component and the *Y* component of the electric field are approximately Gaussian, for both sheaths and ICMEs. The approximately lognormal distribution of the magnetic field strength at 1 AU was initially reported by *Burlaga and King* [1979]. Furthermore, *Burlaga and Lazarus* [2000] examined the distributions of the speed, density, and proton temperature at 1 AU, and the results suggested that the lognormal distribution provides a good model of the observed distributions for 1996–1998. The lognormal distributions suggest the presence of nonlinear interactions and multiplicative dynamical processes, which are manifested in the tail of the distribution [*Burlaga and Ness*, 1998]. The fluctuations of sheath and ICME variables might be associated with the large-scale coronal expansion as well as local nonlinear effects. In fact, the lognormal distribution was also shown to be true for some CME parameters, such as the CME speed near the Sun [*Yurchyshyn et al.*, 2005].

[17] On the average, the magnetic field strength, the *Bz* component, the speed, the density, the proton temperature, the dynamic pressure, the plasma $\beta$, and the Mach number for the sheaths are 15, 80, 4, 60, 70, 62, 67, and 30% higher than the corresponding values for ICMEs, respectively, whereas the *Y* component of the electric field for the sheaths is almost half of that for ICMEs. However, the Gaussian distribution curves of *Ey* for the sheaths and ICMEs are very similar (see Figure 1g), which is consistent with *Pulkkinen et al.* [2007]. According to *Gopalswamy* [2008], the *Dst* index is well correlated with the product *VBz* (equivalent of *Ey*). This indicates that the two structures are equally geoeffective.

[18] *Mitsakou et al.* [2009] examined the correlation between the mean characteristic properties of the ICMEs and sheaths during the descending phase of cycle 23 and found that there is a strong correlation between the sheath and ICME speeds and a medium correlation between the sheath and the ICME magnetic field strength, the proton density, the length scale, and the passage time, while there appears to be no correlation between their temperatures and plasma beta parameters. The strong correlation between the sheath and ICME speeds implies that the shock and ICME are tightly coupled at 1 AU, and the shock is not running away from the ICME, which was first discussed by *Gopalswamy* [2004].

[19] By comparing the normalized occurrence distributions of solar-wind–magnetosphere coupling functions between the sheaths and ICMEs, we found that the two structures have almost equal energy transfer efficiency and a comparable Newell parameter, whereas they show statistically meaningful differences in the dayside reconnection rate according to the Borovsky function.

[20] Because of the comparable energy transfer efficiency for sheaths and ICMEs, we can conclude that the relative contributions to the total energy input into the magnetosphere during these storms are dependent on the amount of time spent within each of the two structures, which is consistent with *Zhang et al.* [2008]. It should be noted, however, that the epsilon parameter seems to suffer from overestimations when pushed to the extreme circumstances [*Rosenqvist et al.*, 2006]. The recent analyses of energy output suggested that we can use epsilon by scaling the parameter up by a factor of 1.5 to 2 when evaluating the energy input into the magnetosphere during intense storms. Moreover, we also should note that the epsilon parameter does not account for all energy passing through the magnetosphere but only that part which is consumed in the storm processes [*Koskinen and Tanskanen*, 2002].

[21] Our results show that the Gaussian distribution curves of the dawn-to-dusk electric fields *Ey* for the sheaths and ICMEs are very similar (see Figure 1g). However, the significant differences in the Borovsky parameter between sheaths and ICMEs are exhibited in Figure 3d. This indicates that, although the solar wind largely controls the rate of the dayside reconnection, the solar-wind control is not directly via the dawn-to-dusk electric field of the solar wind; rather, there is a more complicated control that involves other solar-wind parameters, such as solar-wind pressure and Mach number [*Borovsky*, 2008]. According to the findings of *Borovsky et al.* [2008], the solar-wind electric field $E = -V \times B$ is, at best, an indirect driver: indirect in that $V$ and $B$ of the solar wind in part determine the relevant local plasma parameters at the magnetopause. On the other hand, the differences in dayside reconnection between sheaths and ICMEs could be responsible for the differences in geomagnetic storms driven by ICMEs and sheath regions, which have been reported in prior research. For instance, the sheath-driven storms have stronger auroral activity, stronger magnetotail field stretching, larger asymmetry in the inner magnetosphere field configuration, and a larger asymmetric ring current, while the ring current

enhancement is stronger in the storms driven by magnetic clouds [*Huttunen et al.*, 2002, 2006; *Pulkkinen et al.*, 2007].

[22] **Acknowledgments.** We acknowledge the use of data from the OMNI solar-wind database, complied by the Space Physics Data Facility at Goddard Space Center. This work is jointly supported by the National Natural Science Foundation of China (40890162, 40921063, and 40904049), the 973 Program under grant 2006CB806304, the Knowledge Innovation Program of the Chinese Academy of Sciences and the Specialized Research Fund for State Key Laboratories, and the National Science Foundation for Post-doctoral Scientists of China (20090450589).

[23] Philippa Browning thanks David Webb and another reviewer for their assistance in evaluating this paper.

## References

Akasofu, S.-I. (1981), Energy coupling between the solar wind and the magnetosphere, *Space Sci. Rev.*, *28*, 121–190.

Borovsky, J. E. (2008), The rudiments of a theory of solar wind/magnetosphere coupling derived from first principles, *J. Geophys. Res.*, *113*, A08228, doi:10.1029/2007JA012646.

Borovsky, J. E., and M. H. Denton (2006), Differences between CME-driven storms and CIR-driven storms, *J. Geophys. Res.*, *111*, A07S08, doi:10.1029/2005JA011447.

Borovsky, J. E., M. Hesse, J. Birn, and M. M. Kuznetsova (2008), What determines the reconnection rate at the dayside magnetosphere?, *J. Geophys. Res.*, *113*, A07210, doi:10.1029/2007JA012645.

Burlaga, L. F., and J. H. King (1979), Intense interplanetary magnetic fields observed by geocentric spacecraft during 1963–1975, *J. Geophys. Res.*, *84*(A11), 6633–6640, doi:10.1029/JA084iA11p06633.

Burlaga, L. F., and A. J. Lazarus (2000), Lognormal distributions and spectra of solar wind plasma fluctuations: Wind 1995–1998, *J. Geophys. Res.*, *105*(A2), 2357–2364, doi:10.1029/1999JA900442.

Burlaga, L. F., and N. F. Ness (1998), Magnetic field strength distributions and spectra in the heliosphere and their significance for cosmic ray modulation: Voyager 1, 1980–1994, *J. Geophys. Res.*, *103*(A12), 29,719–29,732, doi:10.1029/98JA02682.

Burlaga, L. F., E. Sittler, F. Mariani, and R. Schwenn (1981), Magnetic loop behind an interplanetary shock: Voyager, Helios, and IMP 8 observations, *J. Geophys. Res.*, *86*(A8), 6673–6684, doi:10.1029/JA086iA08p06673.

Burlaga, L. F., R. M. Skoug, C. W. Smith, D. F. Webb, T. H. Zurbuchen, and A. Reinard (2001), Fast ejecta during the ascending phase of solar cycle 23: ACE observations, 1998–1999, *J. Geophys. Res.*, *106*(A10), 20,957–20,977, doi:10.1029/2000JA000214.

Cane, H. V., and I. G. Richardson (2003), Interplanetary coronal mass ejections in the near-Earth solar wind during 1996–2002, *J. Geophys. Res.*, *108*(A4), 1156, doi:10.1029/2002JA009817.

Gopalswamy, N. (2004), A global picture of CMEs in the inner heliosphere, in *The Sun The Heliosphere as an Integrated System*, edited by G. Poletto and S. Suess, p. 201, Springer, New York.

Gopalswamy, N. (2006), Interplanetary coronal mass ejections, *Space Sci. Rev.*, *124*, 145–168.

Gopalswamy, N. (2008), Solar connections of geoeffective magnetic structures, *J. Atmos. Sol. Terr. Phys.*, *70*, 2078–2100, doi:10.1016/j.jastp.2008.06.010.

Gopalswamy, N., S. Akiyama, S. Yashiro, G. Michalek, and R. P. Lepping (2008), Solar sources and geospace consequences of interplanetary magnetic clouds observed during solar cycle 23, *J. Atmos. Sol. Terr. Phys.*, *70*, 245–253.

Gopalswamy, N., H. Xie, P. Mäkelä, S. Akiyama, S. Yashiro, M. L. Kaiser, R. A. Howard, and J.-L. Bougeret (2010), Interplanetary shocks lacking type II radio bursts, *Astrophys. J.*, *710*, 1111–1126.

Gosling, J. T. (1990), Coronal mass ejections and magnetic flux ropes in interplanetary space, in *Physics of Magnetic Flux Ropes*, *Geophys. Monogr. Ser.*, vol. 58, edited by E. R. Priest, L. C. Lee, and C. T. Russell, pp. 343–364, AGU, Washington, D. C.

Gosling, J. T., R. M. Skoug, D. J. McComas, and C. W. Smith (2005), Direct evidence for magnetic reconnection in the solar wind near 1 AU, *J. Geophys. Res.*, *110*, A01107, doi:10.1029/2004JA010809.

Howard, T. A., amd S. J. Tappin (2005), Statistical survey of Earthbound interplanetary shocks, associated coronal mass ejections and their space weather consequences, *Astron. Astrophys.*, *440*, 373–383.

Huttunen, K. E. J., H. E. J. Koskinen, and R. Schwenn (2002), Variability of magnetospheric storms driven by different solar wind perturbations, *J. Geophys. Res.*, *107*(A7), 1121, doi:10.1029/2001JA900171.

Huttunen, K. E. J., H. E. J. Koskinen, A. Karinen, and K. Mursula (2006), Asymmetric development of magnetospheric storms during magnetic clouds and sheath regions, *Geophys. Res. Lett.*, *33*, L06107, doi:10.1029/2005GL024894.

Huttunen, K. E. J., S. P. Kilpua, A. Pulkkinen, A. Viljanen, and E. Tanskanen (2008), Solar wind drivers of large geomagnetically induced currents during the solar cycle 23, *Space Weather*, *6*, S10002, doi:10.1029/2007SW000374.

Koskinen, H. E. J., and E. Tanskanen (2002), Magnetospheric energy budget and the epsilon parameter, *J. Geophys. Res.*, *107*(A11), 1415, doi:10.1029/2002JA009283.

Lavraud, B., and J. E. Borovsky (2008), Altered solar wind-magnetosphere interaction at low Mach numbers: Coronal mass ejections, *J. Geophys. Res.*, *113*, A00B08, doi:10.1029/2008JA013192.

Lepping, R. P., D. B. Berdichevsky, C.-C. Wu, A. Szabo, T. Narock, F. Mariani, A. J. Lazarus, A. J. Quivers (2006), A summary of WIND magnetic clouds for years 1995–2003: Model-fitted parameters, associated errors and classifications, *Ann. Geophys.*, *24*(1), 215–245.

Lepri, S. T., T. H. Zurbuchen, L. A. Fisk, I. G. Richardson, H. V. Cane, and G. Gloeckler (2001), Iron charge distribution as an identifier of interplanetary coronal mass ejections, *J. Geophys. Res.*, *106*(A12), 29,231–29,238, doi:10.1029/2001JA000014.

Liu, Y., J. D. Richardson, and J. W. Belcher (2005), A statistical study of the properties of interplanetary coronal mass ejections from 0.3 to 5.4 AU, *Planet. Space Sci.*, *53*, 3–17, doi:10.1016/j.pss.2004.09.023.

Mitsakou, E., G. Babasidis, X. Moussas (2009), Interplanetary coronal mass ejections during the descending cycle 23: Sheath and ejecta properties comparison, *Adv. Space Res.*, *43*, 495–498.

Mood, A. M., F. A. Graybill, and D. C. Boes (1974), *Introduction to the Theory of Statistics*, 3rd ed., p. 540, McGraw-Hill, New York.

Neugebauer, M., and R. Goldstein (1997), Particle and field signatures of coronal mass ejections in the solar wind, in *Coronal Mass Ejections*, *Geophys. Monogr. Ser.*, vol. 99, edited by N. Crooker, J. A. Joselyn, and J. Feynman, pp. 245–251, AGU, Washington, D. C.

Newbury, J. A., C. T. Russell, J. L. Phillips, and S. P. Gary (1998), Electron temperature in the ambient solar wind: Typical properties and a lower bound at 1 AU, *J. Geophys. Res.*, *103*(A5), 9553–9566, doi:10.1029/98JA00067.

Newell, P. T., T. Sotirelis, K. Liou, C.-I. Meng, and F. J. Rich (2007), A nearly universal solar wind-magnetosphere coupling function inferred from 10 magnetospheric state variables, *J. Geophys. Res.*, *112*, A01206, doi:10.1029/2006JA012015.

Oh, S. Y., Y. Yi, and Y. H. Kim (2007), Solar cycle variation of the interplanetary forward shock drivers observed at 1 AU, *Sol. Phys.*, *245*, 391–410.

Owens, M. J., P. J. Cargill, C. Pagel, G. L. Siscoe, and N. U. Crooker (2005), Characteristic magnetic field and speed properties of interplanetary coronal mass ejections and their sheath regions, *J. Geophys. Res.*, *110*, A01105, doi:10.1029/2004JA010814.

Padhye, N. E., C. W. Smith, and W. H. Matthaeus (2001), Distribution of magnetic field components in the solar wind plasma, *J. Geophys. Res.*, *106*(A9), 18,635–18,650, doi:10.1029/2000JA000293.

Perreault, P., and S.-I. Akasofu (1978), A study of geomagnetic storms, *Geophys. J. R. Astron. Soc.*, *54*, 547–573.

Pulkkinen, T. I., N. Partamies, K. E. J. Huttunen, G. D. Reeves, and H. E. J. Koskinen (2007), Differences in geomagnetic storms driven by magnetic clouds and ICME sheath regions, *Geophys. Res. Lett.*, *34*, L02105, doi:10.1029/2006GL027775.

Richardson, I. G., and H. V. Cane (1995), Regions of abnormally low proton temperature in the solar wind (1965–1991) and their association with ejecta, *J. Geophys. Res.*, *100*(A12), 23,397–23,412, doi:10.1029/95JA02684.

Richardson, I. G., and H. V. Cane (2004), Identification of interplanetary coronal mass ejections at 1 AU using multiple solar wind plasma composition anomalies, *J. Geophys. Res.*, *109*, A09104, doi:10.1029/2004JA010598.

Riley, P., C. S. Chatzman, H. V. Cane, I. G. Richardson, and N. Gopalswamy (2006), On the rates of coronal mass ejections: remote solar and in situ observations, *Astrophys. J.*, *47*, 648.

Rosenqvist, L., S. Buchert, H. Opgenoorth, A. Vaivads, and G. Lu (2006), Magnetospheric energy budget during huge geomagnetic activity using Cluster and ground-based data, *J. Geophys. Res.*, *111*, A10211, doi:10.1029/2006JA011608.

Skoug, R. M., W. C. Feldman, J. T. Gosling, D. J. McComas, and C. W. Smith (2000), Solar wind electron characteristics inside and outside coronal mass ejections, *J. Geophys. Res.*, *105*(A10), 23,069–23,064, doi:10.1029/2000JA000017.

Tidman, D. A., and N. A. Krall (1971), *Shock Waves in Collisionless Plasmas*, Interscience, Hoboken, N J.

Whang, Y. C. (1977), Probability distribution function of mesoscale magnetic fluctuations during quiet conditions, *Sol. Phys.*, *53*, 507–517.

Wimmer-Schweingruber, R. F., et al. (2006), Understanding interplanetary coronal mass ejection signatures, *Space Sci. Rev.*, *123*, 177–216.

Yurchyshyn, V., S. Yashiro, V. Abramenko, H. Wang, and N. Gopalswamy (2005), Statistical distributions of speeds of coronal mass ejections, *Astrophys. J.*, *619*, 599–603.

Zhang, J., et al. (2007), Solar and interplanetary sources of major geomagnetic storms ($Dst \leq -100$ nT) during 1996–2005, *J. Geophys. Res.*, *112*, A10102, doi:10.1029/2007JA012321.

Zhang, J., W. Poomvises, and I. G. Richardson (2008), Sizes and relative geoeffectiveness of interplanetary coronal mass ejections and the preceding shock sheaths during intense storms in 1996–2005, *Geophys. Res. Lett.*, *35*, L02109, doi:10.1029/2007GL032045.

Zurbuchen, T. H., and I. G. Richardson (2006), In-situ solar wind and magnetic field signatures of interplanetary coronal mass ejections, *Space Sci. Rev.*, *123*, 31–43.

X. Feng, J. Guo, C. Xiang, and P. Zuo, SIGMA Weather Group, State Key Laboratory of Space Weather, Center for Space Science and Applied Research, Chinese Academy of Sciences, 1 Nanertiao, Zhongguancun, Haidian District, Beijing 100190, China. (fengx@spaceweather.ac.cn; jpguo@spaceweather.ac.cn; cqxiang@spaceweather.ac.cn; pbzuo@spaceweather.ac.cn)

Z. Zhang, Department of Computational and Data Sciences, George Mason University, 4400 University Dr., MSN 6A2, Fairfax, VA 22030, USA. (jzhang7@gmu.edu)